applied sciences

MDPI

Article

Numerical Simulation of the Effect of Injected CO_2 Temperature and Pressure on CO_2-Enhanced Coalbed Methane

Hou Yudong [1,2], Huang Saipeng [2], Han Jian [1], Liu Xingbin [1], Han Lianfu [1,*] and Fu Changfeng [1,*]

[1] College of Electronics Science, Northeast Petroleum University, Daqing 163318, China; houyudongzzz@126.com (H.Y.); han-jian@126.com (H.J.); dlts_liuxb@petrochina.com.cn (L.X.)

[2] Key Laboratory of continental shale hydrocarbon accumulation and efficient development of Ministry of Education, Northeast Petroleum University, Daqing 163318, China; huangspcugb@hotmail.com

* Correspondence: Lianfuhan@nepu.edu.cn (H.L.); Changfengfu@nepu.edu.cn (F.C.); Tel.: +86-198-4592-5779 (H.L.); +86-158-4582-8703 (F.C.)

Received: 9 January 2020; Accepted: 15 February 2020; Published: 19 February 2020

Abstract: The injection of CO_2 to displace CH_4 in coal seams is an effective method to exploit coalbed methane (CBM), for which the CO_2 injection temperature and pressure are important influential factors. We performed simulations, using COMSOL Multiphysics to determine the effect of CO_2 injection temperature and pressure on CO_2-enhanced coalbed methane (CO_2-ECBM) recovery, according to adsorption/desorption, seepage, and diffusion of binary gas (CO_2 and CH_4) in the coal seam, and deriver a thermal–hydraulic–mechanical coupling equation of CO_2-ECBM. The simulation results show that, as CO_2 injection pressure in CO_2-ECBM increases, the molar concentration and displacement time of CH_4 in the coal seam significantly decrease. With increasing injection temperature, the binary gas adsorption capacity in the coal seam decreases, and CO_2 reserves and CH_4 production decrease. High temperatures are therefore not conducive for CH_4 production.

Keywords: coalbed methane; CO_2-ECBM; thermal–hydraulic–mechanical; temperature; pressure

1. Introduction

Coalbed methane (CBM) in coal seams is usually stored as free gas in cracks and pores and adsorbed gas on organic surfaces [1]. CBM production not only eliminates the threat of hazardous coal mine production and prevents gas over-limits, but also offers economic benefits [2,3]. CO_2 is a major greenhouse gas and the biggest contributor to climate change [4–8], because its adsorption capacity is higher than that of CH_4. CO_2 displacement can be adopted for CBM recovery [9]. CO_2-enhanced coalbed methane (CO_2-ECBM) technology involves the injection of CO_2 into a coal seam rich in CBM, to sequester CH_4, promotes clean green energy, and is widely used in the production of deep ultra-low permeability coal seams [10–14].

Dell reported that CH_4 could be effectively extracted from crushed coal by injecting flowing CO_2 at ambient temperature [15]. Gentzis injected CO_2 waste from CBM power plants into a coal seam and produced more CH_4, obtaining a competitive adsorption CH_4:CO_2 ratio of approximately 2:1 [16]. Robertson and Christiansen found that H_2S, CO_2, CH_4, and N_2 expand to different degrees in coal seams, and the strain caused by CO_2 adsorption was the largest [17]. Charrière conducted CH_4 and CO_2 adsorption experiments on coal at different temperatures and found that the equilibrium time of coal adsorption of CH_4 and CO_2 is negatively correlated with pressure and temperature and that matrix expansion leads to a decrease of pore width within coal seam fractures [18]. This leads to a significant decrease in permeability. The degree of coal expansion caused by CO_2 is greater than that caused by CH_4 [19]. Wei established a multi-component gas diffusion kinetic model based

on a Bidisperse diffusion mechanism and Maxwell–Stefan (MS) diffusion theory to verify model effectiveness under pure gas diffusion conditions [20]. Fujioka studied the feasibility of storing CO_2 underground while extracting CH_4 from coal seams and showed that CO_2 injection can increase gas production [21]. The results of Luo showed that vertical permeability heterogeneity can improve the transport capacity of CO_2 to a production well [22]. Vishal used numerical simulations to study the production effect of coal with different sorption times under CO_2 action. Their results indicate that the CO_2 injection capacity of coal with high sorption time is higher than that of coal with low sorption time [23]. Wang established a fully coupled gas flow model based on double permeability diffusion, adsorption strain, and geomechanics and showed that the double-pore diffusion model better describes the diffusion process than the single-pore diffusion model [24]. Fan established the hydraulic–mechanical–thermal coupling model of CO_2-ECBM, considering the diffusion of CO_2 and CH_4 gas and non-isothermal initial temperature absorption of coal, and simulated the effect of injection pressure and initial reservoir temperature on CO_2-ECBM [25]. Fang established a fully coupled equation of gas diffusion, adsorption, seepage, and heat transfer and simulated the displacement process and effective influence radius of injected CO_2 under different pressure and temperature conditions [26].

The abovementioned studies on CO_2-ECBM established the developmental foundation CBM displacement by CO_2. However, most scholars have assumed a single temperature or pressure parameter in the study of numerical simulation of CO_2-ECBM, and most of them set the coal seam as a homogeneous body. In this paper, we established the THM coupling equation of CO_2-ECBM for coal seams with non-uniform porosity and that are non-isothermal, and non-isobaric adsorption of binary gas is considered while combining percolation and diffusion. To study the effects on gas recovery and coal seam permeability, we used COMSOL Multiphysics to simulate the process of injecting CO_2 with different pressures and temperatures to displace coalbed methane.

2. Theory

2.1. Desorption–Seepage–Diffusion Principle of CO_2 Displacement of CH_4

The CO_2 adsorption capacity of coal seams is greater than that of CH_4. After injecting CO_2 into a coal seam, adsorption competes with CH_4 and some of the latter is simultaneously displaced. The injection of CO_2 increases the energy of the coal seam and produces a partial pressure effect on the adsorption of CH_4, which reduces the adsorption pressure of CH_4 and promotes its desorption. After desorption, CO_2 changes from an adsorbed state to a free state. Gas molecules diffuse under a concentration and pressure gradient, migrating from higher concentration to lower concentration and then to the wellbore of the production well.

2.2. THM Coupling Equation of CO_2 Displacement CBM

The process of CO_2 displacement of CBM mainly involves THM coupling, as shown in Figure 1. We therefore establish a THM-coupling model of deformation, heat transfer, gas adsorption/desorption, seepage, and diffusion of coal with a heterogeneous porous medium. The field equation is based on the following assumptions:

(1) The coal seam is a heterogeneous porous medium;
(2) The binary gas adsorption and desorption models conform to the Langmuir equation [27];
(3) The influence of water and vapor on gas transport is not considered [28];
(4) The free-state carbon dioxide and methane gas in the coal seam obey the ideal gas state equation (ignoring the influence of gas compression coefficient and temperature on gas viscosity) [25–27,29–31];
(5) The migration mode of binary gas in the coal seam pores obeys Fick diffusion law, the free binary gas transport in coal seam obeys Darcy's law, and binary gas mass exchange occurs between diffusion and seepage [16,32];

(6) The initial state of the coal seam's only free adsorption state of CBM sets CO_2 content to 0 with binary gas in the boundary around the coal seam as no flux.

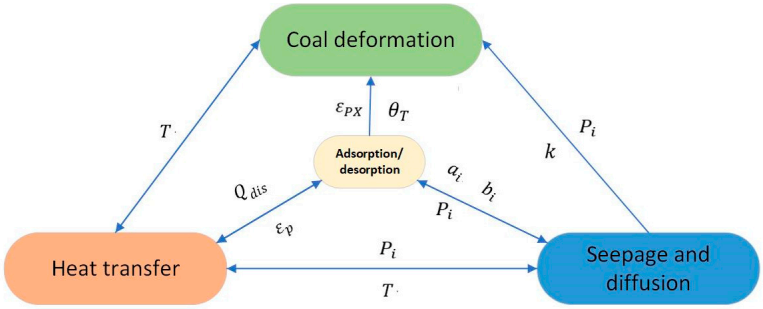

Figure 1. Schematic diagram of the full coupling of THM for CO_2 displacement CBM.

2.2.1. Stress–Strain Equation

The coal seam is a heterogeneous porous medium model. The deformation field of coal seam is affected by pore pressure, temperature, and matrix expansion caused by gas adsorption and desorption. The stress is expressed as the strain equation [25,33–36]:

$$\varepsilon_{ij} = \frac{1}{2G}\delta_{ij} - (\frac{1}{6G} - \frac{1}{9K})\sigma_{kk}\delta_{ij} + \varepsilon_{PY}\delta_{ij} + \varepsilon_T\delta_{ij} + \varepsilon_{PX}\delta_{ij} \quad (1)$$

where G is the shear modulus (Pa); K is the bulk modulus of coal (Pa); ε_{PY} is gas strain; ε_T is thermal expansion strain; and ε_{PX} is the strain caused by gas pressure. The equation is as follows:

$$\begin{cases} G = \dfrac{E}{2(1+v)} \\ K = \dfrac{E}{3(1-2v)} \\ \varepsilon_{PY} = -\dfrac{\alpha\Delta P}{3K_s} \\ \varepsilon_T = \dfrac{\beta\Delta T}{3} \\ \varepsilon_{PX} = \dfrac{2\rho_c RTa_i}{3V_m K}\ln(1+\sum_{i=1}^{2} b_i P_i) \end{cases} \quad (2)$$

where E is the Young's modulus (Pa); v is the Poisson's ratio; β is the thermal expansion coefficient (K^{-1}); V_m is the molar constant of gas; R is the universal gas constant (J/mol·k); δ_{ij} is the Kronecker function; a_i is the Langmuir volume constant (m^3/kg); b_i is the Langmuir pressure constant (Pa^{-1}); P_i is the gas pressure(MPa); ρ_c is the density of coal (kg/m^3); and T is the temperature of the coal (K).

The strain and displacement components satisfy the Cauchy equation [28,37]:

$$\varepsilon_{ij} = \frac{1}{2}\left(u_{ij} + u_{ji}\right) \quad (3)$$

where ε_{ij} is the train component, and u_{ij} is the displacement component.

The equilibrium differential equation of coal seam is defined as the Navier–Stokes equation [28,37]:

$$\sigma_{ij,j} + F_i = 0 \quad (4)$$

The modified equilibrium differential equation is as follows [38]:

$$\sigma'_{ij,j} + \left(\alpha P\sigma_{ij}\right)_{,j} + F_i = 0 \quad (5)$$

Combined with Equations (1)–(5), the coal stress equation is as follows:

$$Gu_{i,jj} + \frac{G}{1-2v}u_{j,ji} + \theta_{PY}\Delta P_{,i} + \theta_T \Delta T_{,i} + \theta_{PX} a_i T\left[\ln(1 + \sum_{i=1}^{2} b_i P_i)\right]_{,i} + \alpha P_{,i} + F_i = 0 \quad (6)$$

where θ_{PY} is the stress coefficient caused by gas pressure, θ_T is the coefficient of thermal stress, θ_{PX} is the stress coefficient caused by gas adsorption, and α is the Biot coefficient. The equation is as follows:

$$\begin{cases} \theta_{PY} = \dfrac{3\lambda - 2G}{3K} \\ \theta_T = \dfrac{3\lambda + 2G}{3}\beta \\ \theta_{PX} = \dfrac{2\rho_c R(3\lambda + 2G)}{3V_m K} \\ \alpha = 1 - K/K_s \\ \lambda = \dfrac{Ev}{(1+v)(1-2v)} \end{cases} \quad (7)$$

where K_S is bulk modulus of coal skeleton, and σ_{ij} is stress tensor (i, j = 1, 2).

2.2.2. Coupling Equation of Permeation and Diffusion of Binary Gas

Gas seepage in coal seams is driven by a pressure gradient and gas gravity is ignored. The gas seepage velocity expression in coal is derived from Darcy's law [25]:

$$q_g = -\frac{KRT}{\mu_i}\nabla c_i \quad (8)$$

where q_g is seepage velocity(m^3/s); $\nabla = \left[\frac{\partial}{\partial x}, \frac{\partial}{\partial y}, \frac{\partial}{\partial z}\right]$; and μ_i is viscosity coefficient of single phase.

Gas diffusion follows Fick's law. Its diffusion flux is expressed as follows [39]:

$$J_i = -D_i \nabla c_i \quad (9)$$

where J_i is the diffusion component of single phase; D_i is the diffusion coefficient of single phase (m^2/s).

CO_2 is injected into coal seams containing CH_4 driven by a pressure gradient, and the flow of binary gas in coal seam conforms to the convection–diffusion equation [25]:

$$\frac{\partial(m_i)}{\partial t} + \nabla \cdot (-\frac{kRT}{\mu_i}\nabla c_i \rho_i) + \nabla \cdot (-D_i \varphi \nabla c_i) = Q_S \quad (10)$$

where i is the single component gas; $i = 1$ is CH_4; $i = 2$ is CO_2; m_i is the gas mass of each component (kg); c_i is the molar concentration of a single component (mol/m^3); ρ_i is the density of a single component (kg/m^3); k is permeability (m^2); φ is porosity; and Q_S is the source term ($kg/(m^3 \cdot s)$).

For the ideal state equation of binary mixed gas, the molar concentration of each gas is expressed as follows [24]:

$$c_i = \frac{P_i}{RT} \quad (11)$$

CO_2 and CH_4 gases exist simultaneously in the coal seam during CO_2 displacement. The mass of the gas is the sum of adsorbed and free gases considering the influence of temperature on the adsorption capacity. The Langmuir adsorption equation can be used to represent the adsorption mass as follows:

$$m_i = \rho_c \rho_a \frac{a_i b_i c_i RT}{1 + \sum_{i=1}^{2} b_i P_i} + \varphi M_i c_i \quad (12)$$

Combined with Equations (8)–(12), the binary gas seepage and diffusion equation can be obtained as follows:

$$\frac{\partial\left(\rho_c\rho_a\frac{a_ib_ic_iRT}{1+\sum_{i=1}^{2}b_iP_i}+\varphi M_ic_i\right)}{\partial t}+\nabla\cdot(-\frac{kRT}{\mu_i}\nabla c_i\rho_i)+\nabla\cdot(-D_i\varphi\nabla c_i)=Q_s \tag{13}$$

2.2.3. Temperature Field Equation of Binary Gas Flow

The system is treated as the thermal equilibrium state, and the coal seam is set as a porous medium of linear thermoelastic material [25]. Deformation work and heat applied to the coal seam are equal to the sum of its kinetic and internal energies. Because deformation of the coal seam is small and reversible, the kinetic energy can be ignored. The energy balance equation of the coal seam is then as follows:

$$\delta Q_H = dU-\delta_{ij}d\varepsilon_{ij}=\rho_cC_VdT+T\frac{\partial\delta_{ij}}{\partial t}d\varepsilon_{ij} \tag{14}$$

where dQ_H is the heat source for thermal expansion, volumetric deformation, and adsorption deformation caused by temperature changes; dU is the internal energy per unit volume; and C_V is specific heat at constant volume of coal seam.

The partial derivative of the thermoelastic physical equation is obtained:

$$\frac{\partial\sigma_{ij}}{\partial t}=\frac{\partial\left[-Q_T\Delta T\delta_{ij}+Q_{PX}\Delta P\delta_{ij}+Q_{PY}a_iT\left[\ln(1+\sum_{i=1}^{2}b_iP_i)\right]\delta_{ij}\right]}{\partial t} \tag{15}$$

Ignoring the influence of water and ash content on the coal seam, the heat source in the coal seam is mainly composed of energy absorbed by gas adsorption, release, and desorption. The heat generated by coal deformation, the gas flow temperature field equation, is as follows:

$$dQ_H=\eta\nabla^2T+Q_{dis} \tag{16}$$

where η is thermal conductivity of coal; $\eta\Delta^2T$ is the change of heat flow into and out of unit volume by heat conduction of gas in unit time; and Q_{dis} is differential heat source.

Because binary gas desorption of the coal seam is a reversible adsorption process, gas desorption in the coal seam changes from an adsorption state to a free state. The expressions of heat absorbed during CH_4 desorption in a coal seam and heat released during CO_2 adsorption are as follows:

$$Q_{\text{dis}}=\frac{\partial\left[\frac{a_ib_iP_i\rho_a\rho_iRT}{M_i(1+\sum_{i=1}^{2}b_iP_i)}\ln\left[\frac{\varphi M_i(1+\sum_{i=1}^{2}b_iP_i)}{a_ib_i\rho_a\rho_iRT}\right]\right]}{\partial t} \tag{17}$$

By combining Equations (14)–(17), the temperature field control equation of binary gas is obtained as follows:

$$\eta\nabla^2T+Q_{dis}=\rho_cC_V\frac{\partial T}{\partial t}+Q_T\Delta T\delta_{ij}\frac{\partial e}{\partial t}+Q_{PX}a_iT\left[\ln(1+\sum\nolimits_{i=1}^{2}b_iP_i)\right]\frac{\partial e}{\partial t} \tag{18}$$

2.2.4. Porosity and Permeability

The adsorption and desorption of gas in the seepage and diffusion field, compression of the stress field on the coal seam, and thermal expansion of the temperature field are transformed into the influence on porosity, which is defined as follows [40]:

$$\varphi=1-\frac{1-\varphi_0}{1+\text{e}}(1+\frac{\Delta V_S}{V_{S0}}) \tag{19}$$

where φ_0 is the initial porosity of coal; e is the volumetric strain of coal; V_{S0} is the initial volume of coal skeleton; ΔV_S is the coal skeleton volume changes under the comprehensive action of pore pressure compression, thermal expansion, and gas absorption expansion.

The effects of gas pressure and coal temperature on porosity are considered:

$$\varphi = 1 - \frac{1-\varphi_0}{1+e}(1 + \frac{\Delta V_{SP}}{V_{S0}} + \frac{\Delta V_{ST}}{V_{S0}}) \tag{20}$$

where ΔV_{SP} is bulk expansion and deformation of coal caused by pressure; ΔV_{ST} is bulk expansion and deformation of coal caused by temperature change, and the equation is as follows:

$$\begin{cases} \frac{\Delta V_{SP}}{V_{S0}} = -\frac{\Delta P}{K_S} \\ \frac{\Delta V_{ST}}{V_{S0}} = \beta \Delta T \end{cases} \tag{21}$$

Volumetric deformation resulting from gas adsorption and desorption is given as follows [41]:

$$\varepsilon_p = \frac{2\rho_c RTa_i}{3V_m K} \ln(1 + \sum\nolimits_{i=1}^{2} b_i P_i) \tag{22}$$

The porosity equation can be obtained by integrating the porosity factors:

$$\varphi = 1 - \frac{1-\varphi_0}{1+e}(1 - K_Y \Delta P + \beta \Delta T + \frac{\frac{2\rho_c RTa_i}{3V_m K} \ln(1 + \sum_{i=1}^{2} b_i P_i)}{1-\varphi_0}) \tag{23}$$

The relationship between porosity, permeability, and particle size distribution in porous media is as follows [29,33]:

$$k = \frac{d_e^2 \varphi^3}{72(1-\varphi)^2} \tag{24}$$

where d_e is the effective diameter of particle. According to Equation (22), we obtain:

$$\frac{k}{k_0} = \left(\frac{\varphi_0}{\varphi}\right)^3 \left(\frac{1-\varphi_0}{1-\varphi}\right)^2 \tag{25}$$

The second term on the right tends to be consistent when porosity is substantially lower than 1. The relationship between porosity and permeability is as follows [42,43]:

$$k = k_0 \left(\frac{\varphi}{\varphi_0}\right)^3 \tag{26}$$

where k_0 is the initial permeability (m^2), and coal seam permeability is as follows:

$$k = k_0 \left(\frac{1 - \frac{1-\varphi_0}{1+e}(1 + \frac{\Delta V_{SP}}{V_{S0}} + \frac{\Delta V_{ST}}{V_{S0}})}{\varphi_0} \right)^3 \tag{27}$$

3. Geometric Model and Solution Conditions

We simplify the CBM reservoir in Northern Sichuan (Qinshui Basin, China) into a two-dimensional model, according to the production block of CO_2 displacement of CH_4 and ignoring the coal seam thickness. The geometric model simplify is simplified to a two-dimensional model of a square area with a side length of 100 m. Considering the symmetry, the 1/4 of the area is selected as a numerical simulation area. As shown in Figure 2, COMSOL Multiphysics software was used to establish a coal seam model with a size of 50 × 50 m. A 1 m diameter production well is located at the bottom right of the model and the pressure is set to 1 atm (0.1 MPa). An injection well with a 1 m diameter is located

in the upper left of the model. A triangular mesh was used to divide into 25,504 cells. To facilitate the observation of simulation results, A (15, 35) and B (35, 15) were set as simulation monitoring points of the model. The initial pressure and temperature of the coal seam are 2 MPa and 273 K, respectively. The coal seam and well boundaries are fixed constraints. The initial porosity of each point is $\varphi_{0(x,y)}$ and the model parameters are listed in Table 1.

Table 1. Numerical simulation parameter [25,26,28].

Variable	Parameter	Value
P_0	Gas pressure under standard conditions (MPa)	2
T_0	Initial temperature of coal seam (K)	273
ρ_c	The density of coal (kg/m^3)	1350
M_1	CH_4 molar mass (kg/mol)	0.016
M_2	CO_2 molar mass (kg/mol)	0.044
μ_1	CH_4 dynamic viscosity coefficient (Pa·s)	1.03×10^{-5}
μ_2	CO_2 dynamic viscosity coefficient (Pa·s)	1.38×10^{-5}
ρ_1	CH_4 density under standard conditions (kg/m^3)	0.717
v	Poisson's ratio	0.35
E	Young's modulus of coal (MPa)	2713
R	Universal gas constant (J/(mol·k))	8.314
σ	Thermal conductivity (W/(m·k))	0.478
β	Thermal expansion coefficient (K^{-1})	2.4×10^{-5}
C_p	Heat capacity at constant stress (J/(kg·k)	1000

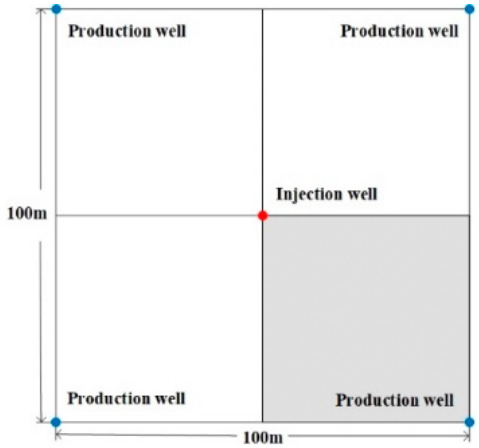

(**a**)

Figure 2. *Cont.*

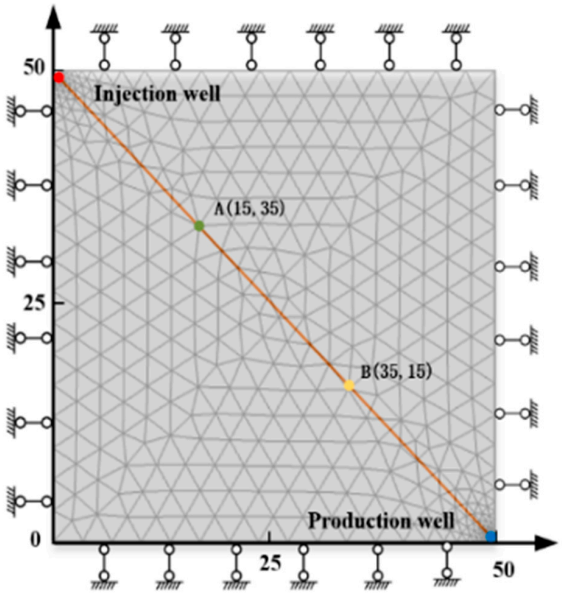

(**b**)

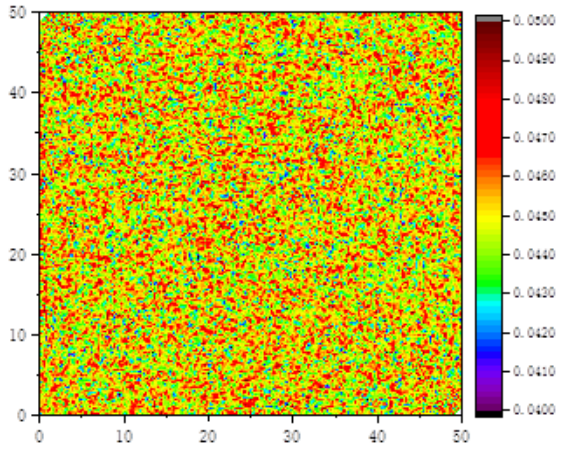

(**c**)

Figure 2. Numerical model of CO_2 displacement of coalbed methane: (**a**) geological model of enhancing CBM recovery by injecting CO_2 with heat injection; (**b**) numerical simulation model for CO_2-ECBM; and (**c**) initial porosity of CO_2-ECBM.

4. Results

4.1. Effect of Injected CO_2 Pressure on CO_2-ECBM

According to [25,26], hydraulic–mechanical–thermal coupled model of CO_2-ECBM can effectively reveal the influence of CO_2 storage on CH_4 production. Therefore, we investigate the distribution rule of CO_2 and CH_4 molar concentrations in CBM over a period of 30 years to study the effect of CO_2 injection pressure on CO_2-ECBM at constant temperature and variable pressure. The injected CO_2 pressures are 4, 6, and 8 MPa, and the initial temperature of the coal seam is 273 K. Figure 3 shows the migration relationship of CH_4 and CO_2 molar concentration with time under injected CO_2 of variable pressure.

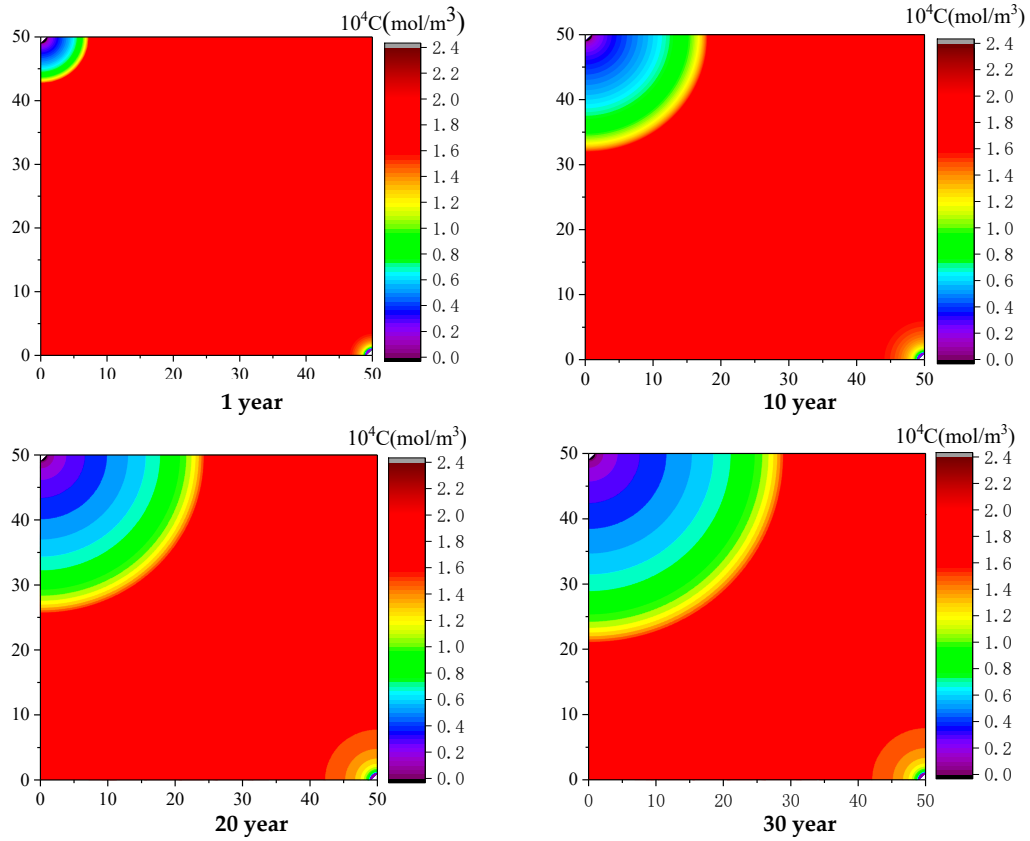

(**a**)

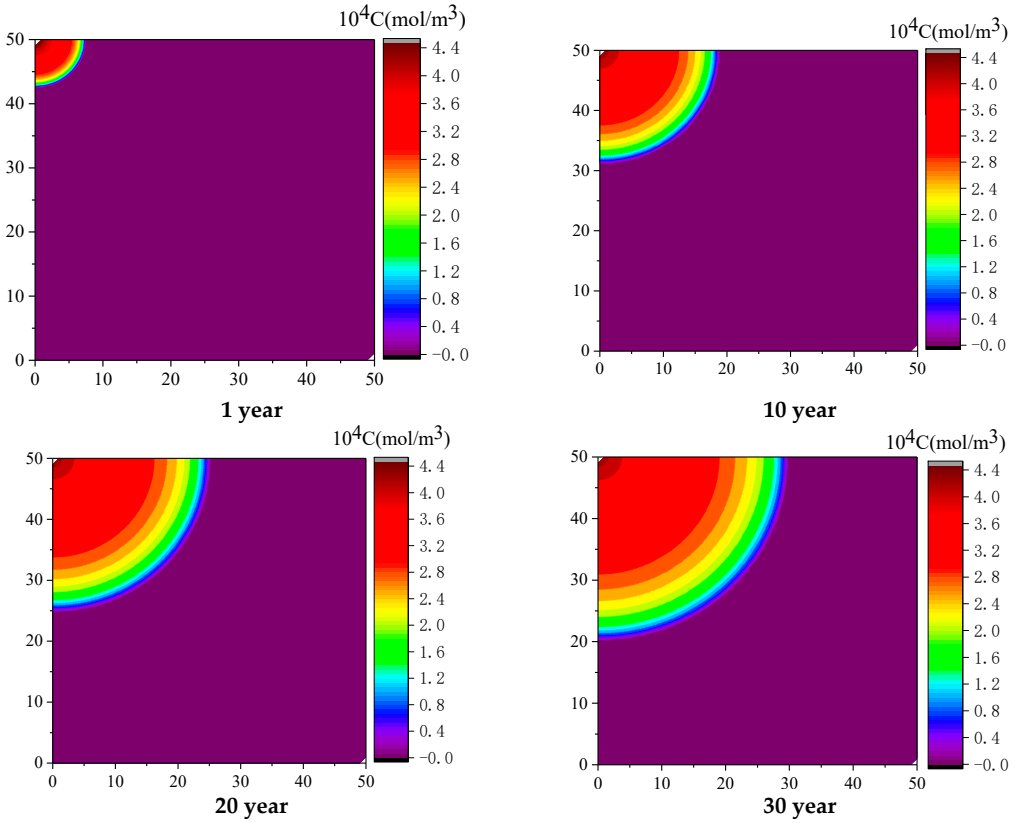

(**b**)

Figure 3. *Cont.*

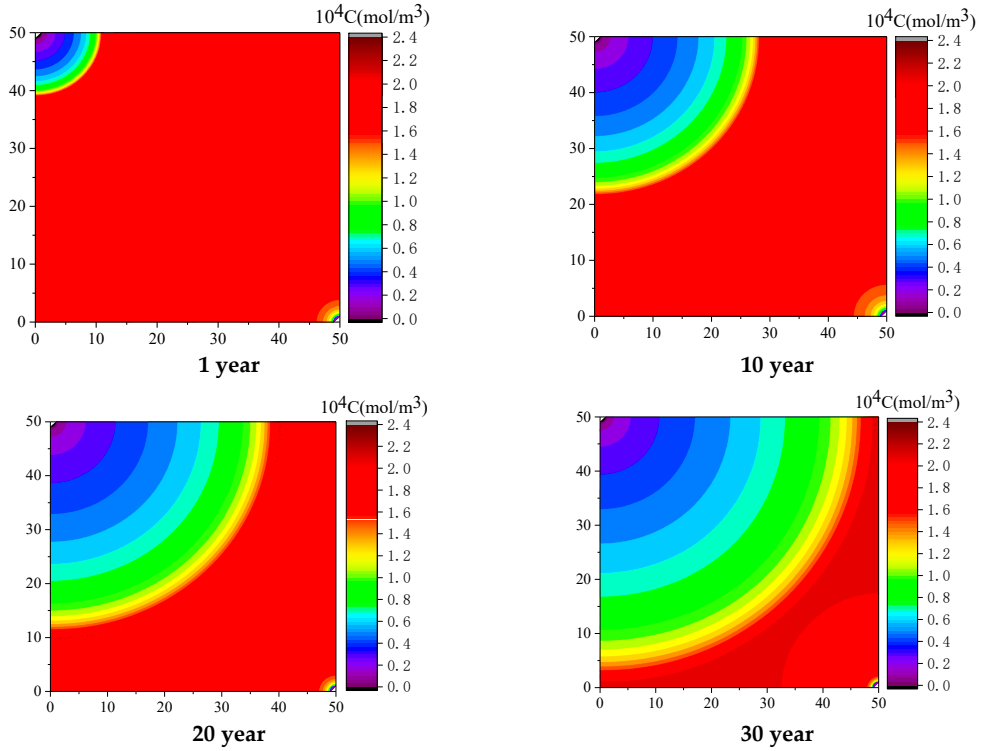

(**c**)

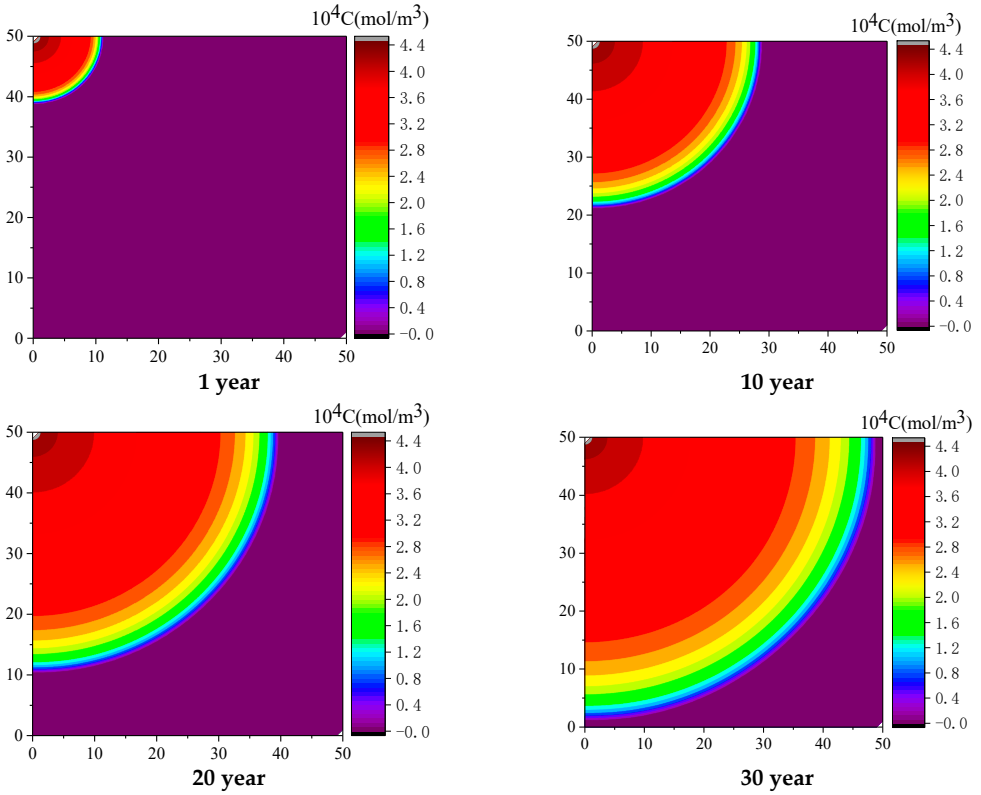

(**d**)

Figure 3. *Cont.*

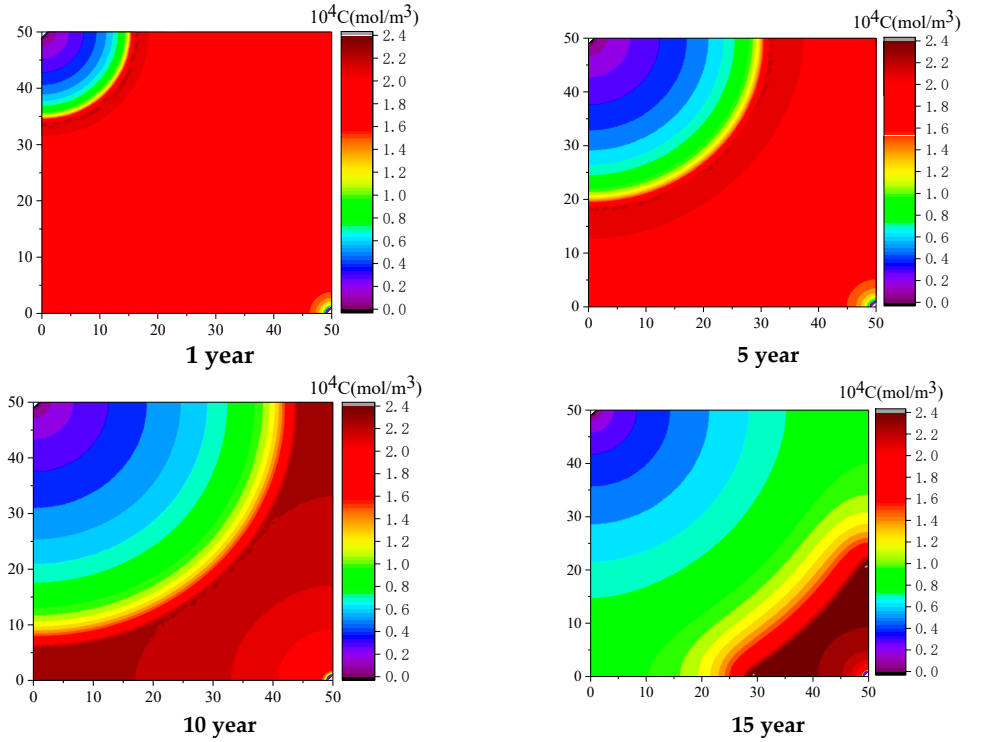

Figure 3. Distribution of CH_4 molar concentration and CO_2 molar concentration under different injection CO_2 pressures: (**a**) distribution of CH_4 molar concentration at 4 MPa injection pressure; (**b**) distribution of CO_2 molar concentration at 4 MPa injection pressure; (**c**) distribution of CH_4 molar concentration at 6 MPa injection pressure; (**d**) distribution of CO_2 molar concentration at 6 MPa injection pressure; (**e**) distribution of CH_4 molar concentration at 8 MPa injection pressure; and (**f**) distribution of CO_2 molar concentration at 8 MPa injection pressure.

Figure 3 shows the migration of CH_4 and CO_2 molar concentration with time under different injected CO_2 pressures. Figure 3a,c,e shows CH_4 molar concentration when the injection pressure is 4, 6, and 8 MPa, respectively. It can be seen that the CO_2 injection pressure significantly affects the displacement and migration rate of CH_4. Moreover, higher CO_2 injection pressures are associated with faster CH_4 migration rates and lower molar concentrations. Figure 3b–f shows the molar concentration of CO_2 when the injection pressure is 4, 6, and 8 MPa, respectively. Increasing the injection pressure and time leads to an increase in influence radius and molar CO_2 concentration in the coal seam. After 30 years of production, when the injection pressure is 4 and 6 MPa, the influence radius of CO_2 is 32 and 55 m, respectively. CO_2 reaches the producing well 17 years after production at an injection pressure of 8 MPa. The results are basically consistent with [25,26].

Figure 4 shows the variation of CH_4 molar concentration per unit volume of the diagonal with time. The CH_4 molar concentration increases from the injection well to the displacement front and reaches the maximum value at the latter. The same results can be obtained from the displacement front to the production well because the displacement front is the area with the greatest gas pressure caused by migration. At a certain point along the diagonal of the model, longer displacement times are associated with low CH_4 molar concentrations, and higher injection pressures are associated with faster CH_4 migration and lower molar concentration. After the injected CO_2 pressure reaches 8 MPa for 30 years, the maximum molar concentration of CH_4 in the coal seam is 1.42×10^3 (mol/m^3), and the production rate is 92%.

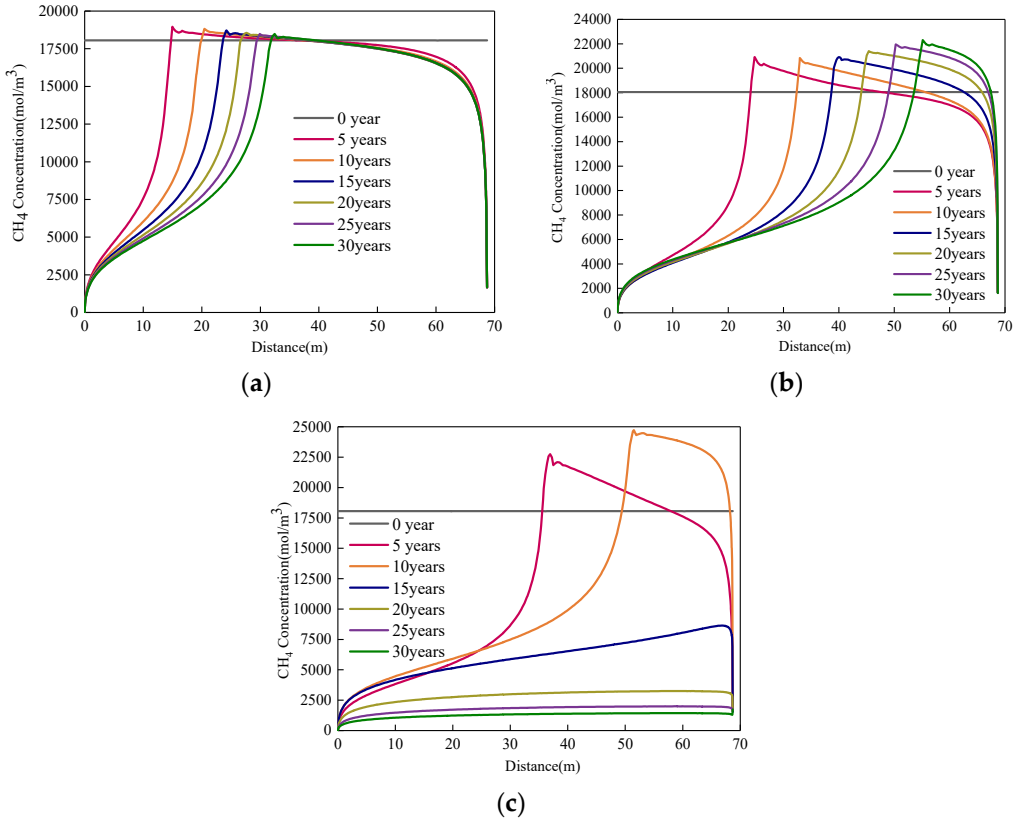

Figure 4. Distribution of diagonal CH_4 molar concentrations at different injection pressures: (**a**) injection pressures is 4 MPa; (**b**) injection pressures is 6 MPa; and (**c**) injection pressures is 8 MPa.

Figure 5 shows the variation of CO_2 molar concentration per unit volume of the diagonal with time. Shorter distances from the injection well are associated with greater amounts of CO_2. There is no CO_2 from the displacement front to the production well. For a certain point along the diagonal,

a longer displacement time and injection pressure lead to more CO_2 entering the coal seam. The results are basically consistent with [27].

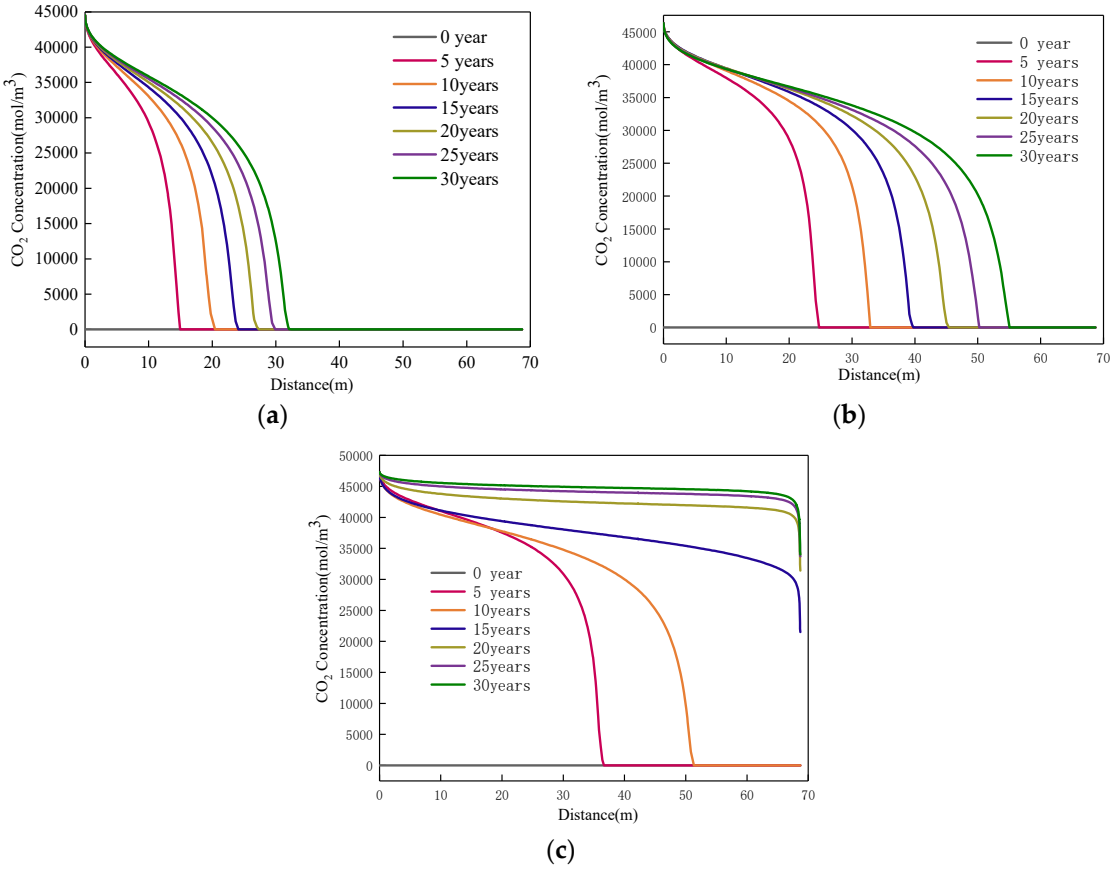

Figure 5. Distribution of diagonal CO_2 molar concentrations at different injection pressures: (**a**) injection pressures is 4 MPa; (**b**) injection pressures is 6 MPa; and (**c**) injection pressures is 8 MPa.

Figure 6a shows the change of CH_4 molar concentration with time at points A and B simultaneously under different CO_2 injection pressures. The CH_4 molar concentration near the injection well A is lower than that far away from the injection well B, and higher injection pressures are associated with higher CH_4 displacement per unit volume. Figure 6b shows the change of CO_2 molar concentration with time at points A and B under different injection pressures. Higher pressures are associated with faster CO_2 migration speeds and higher CO_2 molar concentrations. The displacement occurs first near the injection well. Increasing displacement time shows increased CO_2 molar concentrations in the coal seam.

The above analysis shows that high injection pressures are associated with faster gas seepage in the coal seam. CO_2 reserves and CH_4 production both increase with increasing injected CO_2 pressure.

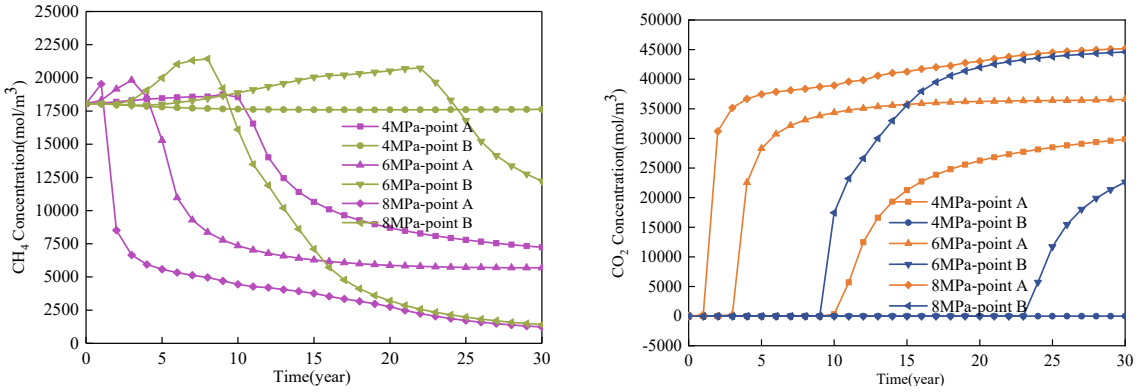

Figure 6. CH_4 and CO_2 molar concentrations at monitoring points A and Bunder different CO_2 injection pressures: (**a**) CH_4 molar concentration and (**b**) CO_2 molar concentration.

4.2. Effect of Injected CO_2 Temperature on CO_2-ECBM

To study the effect of CO_2 injection temperature on CO_2-ECBM, CO_2 with different temperatures is injected into the coal seam at a fixed pressure, and the distribution rule of CO_2 and CH_4 mole concentrations in CBM over 30 years is investigated. The CO_2 injection temperature is 303, 333, and 363 K, and the pressure of the coal seam is 6 MPa. Figure 7 shows the migration relationship of CH_4 and CO_2 molar concentration with time under different CO_2 injection temperatures.

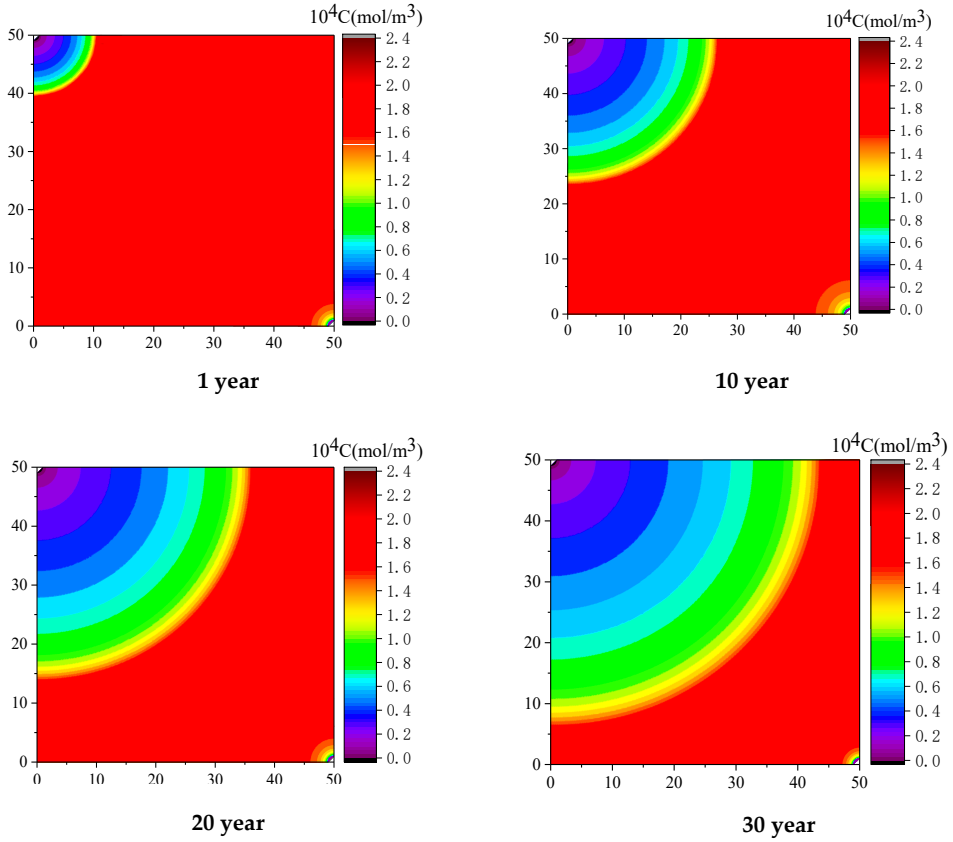

Figure 7. *Cont.*

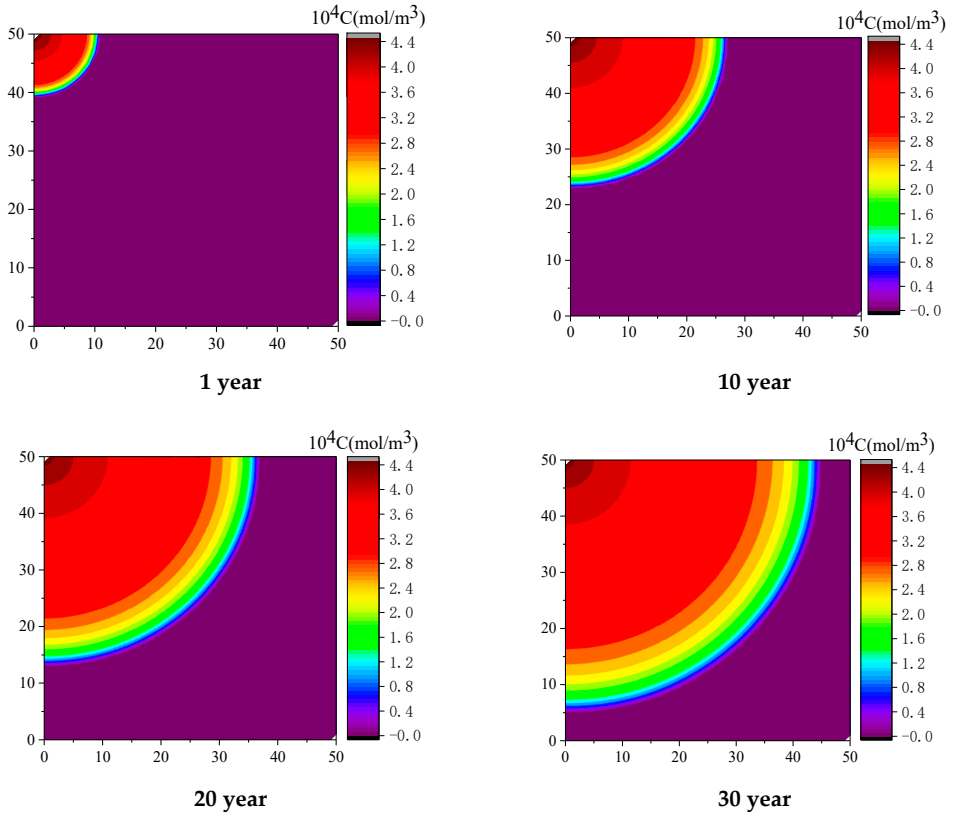

(**b**)

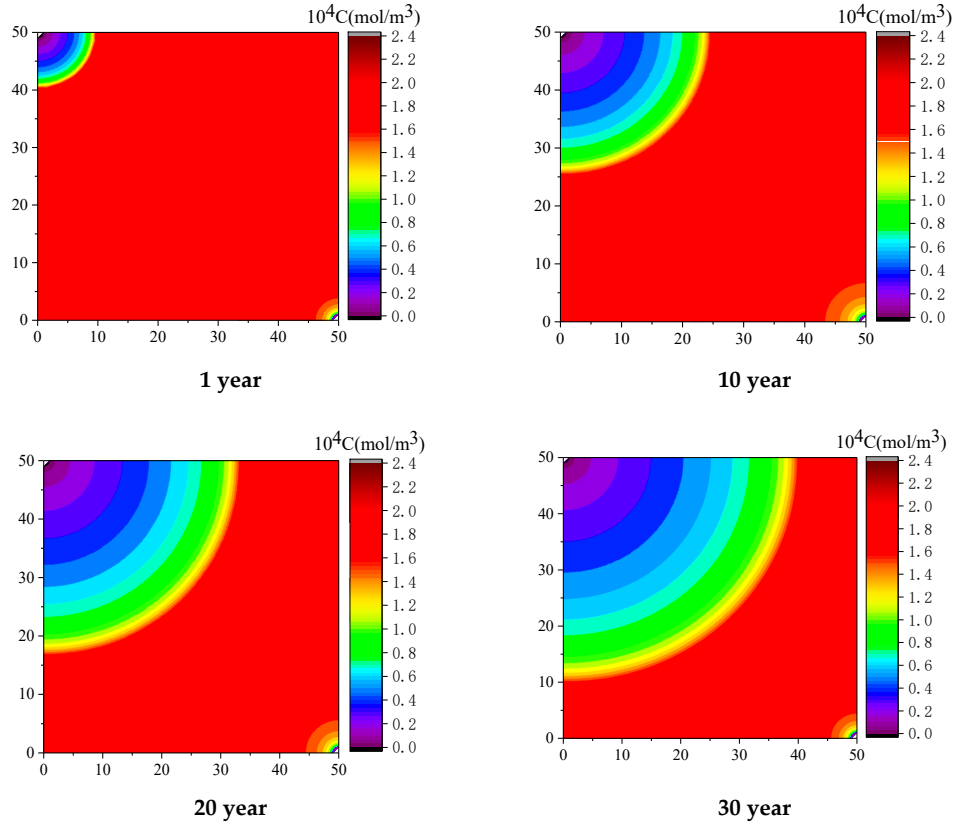

(**c**)

Figure 7. *Cont.*

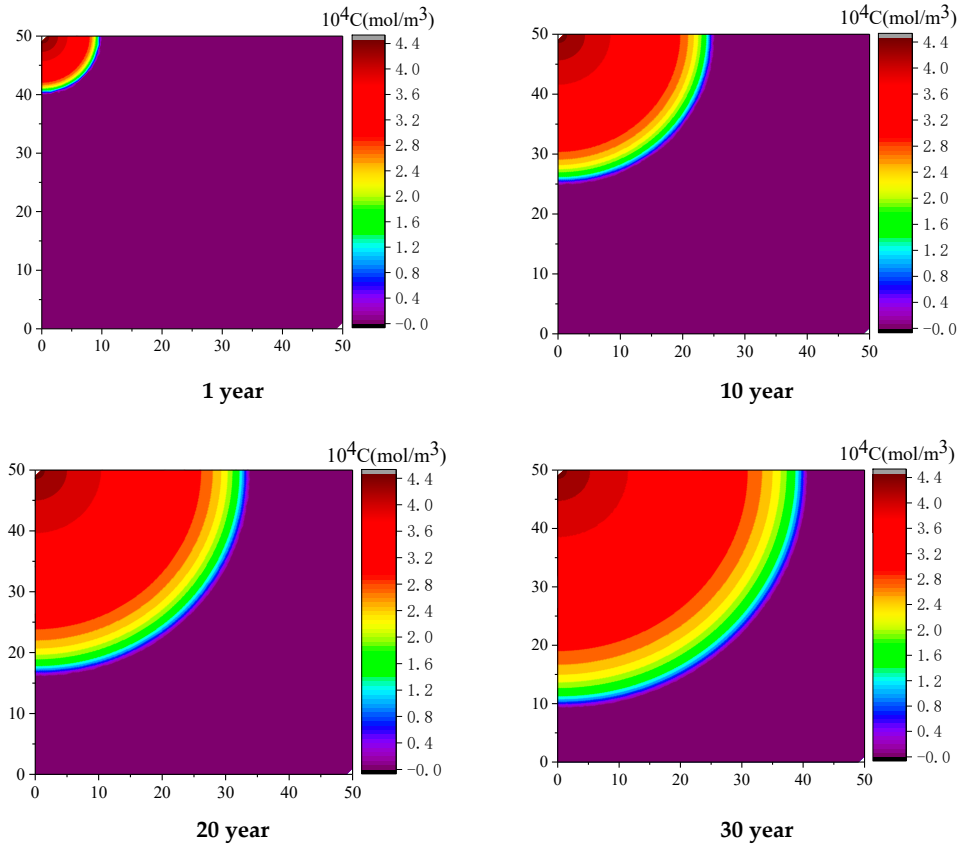

(**d**)

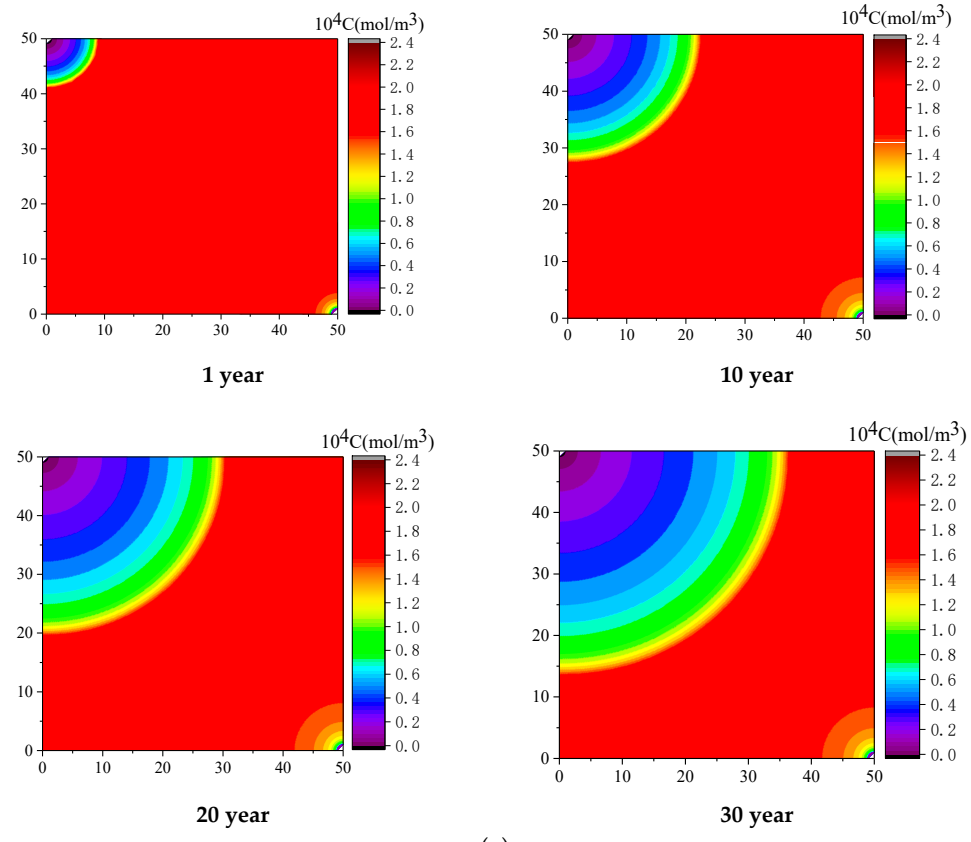

(**e**)

Figure 7. *Cont.*

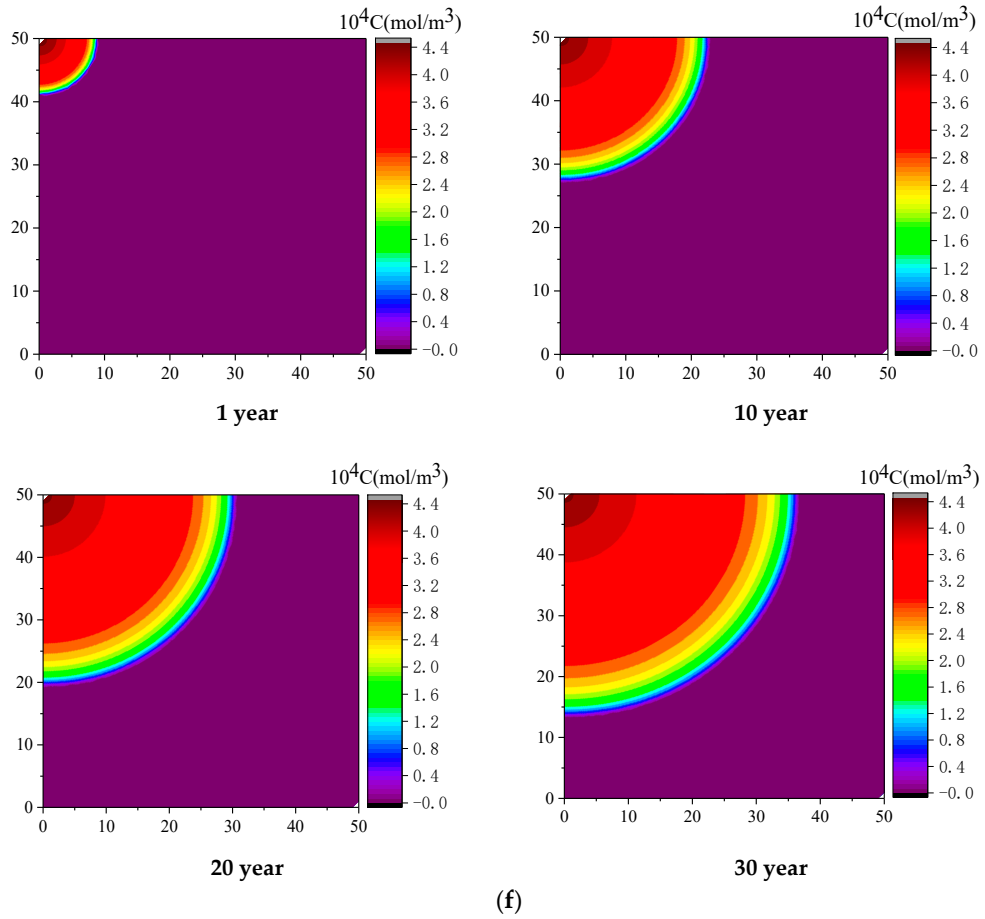

Figure 7. Distribution of CH_4 and CO_2 molar concentrations under different CO_2 injection temperatures: (**a**) distribution of CH_4 molar concentration at 303 K injection temperatures; (**b**) distribution of CO_2 molar concentration at 303 K injection temperatures; (**c**) distribution of CH_4 molar concentration at 333 K injection temperatures; (**d**) distribution of CO_2 molar concentration at 333 K injection temperatures; (**e**) distribution of CH_4 molar concentration at 363 K injection temperatures; and (**f**) distribution of CO_2 molar concentration at 363 K injection temperatures.

Figure 7a,c,e shows the molar concentrations of CH_4 at different temperatures under a CO_2 injection pressure of 6 MPa. The production of CH_4 decreases with increasing injection well temperature. After 30 years of heating injection and production, the displacement radius of CH_4 at high temperature is smaller than that at low temperature. Figure 7b,d,f are the molar concentrations of CO_2 at different temperatures, also under an CO_2 injection pressure of 6 MPa. After 30 years of heating, the diffusion rate of CO_2 decreases with increasing temperature, which makes the molar concentration of CO_2-ECBM lower at a high temperature than that at a low temperature under the same pressure.

Figure 8 shows the molar concentrations of CH_4 and CO_2 at points A and B at different temperatures under a CO_2 injection pressure of 6 MPa. The molar concentration of CH_4 at point A at high temperature is lower than that at low temperature, and the law of the molar concentration of CO_2 at point A is the same as that of CH_4. After 30 years of injection and production, the CH_4 molar concentration at point B is higher at high temperature than at low temperature, while the CO_2 molar concentration is lower than at low temperature. This is because to the coal seam under rising temperature undergoes matrix expansion and decreased permeability. The migration rate of CO_2 decreases owing to the low permeability, which allows it to fully displace CH_4 from the coal seam, but permeability is further reduced at high temperature as a result of CH_4 in the coal seam. The molar concentration of CH_4 production increase is therefore not apparent.

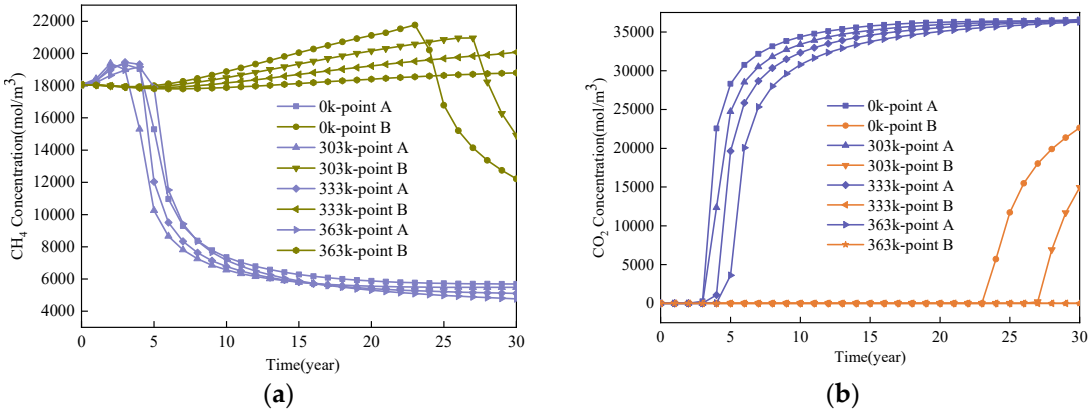

Figure 8. CH_4 and CO_2 molar concentrations at monitoring points A and Bunder different CO_2 injection temperatures: (**a**) CH_4 molar concentration and (**b**) CO_2 molar concentration.

Figure 9 shows the changes in permeability ratio of monitoring points A and B when the CO_2 injection pressure is 4, 6, and 8 MPa. The permeability ratio of monitoring points A and B increases over 40 years when the CO_2 injection pressure is 4 and 6 MPa. When the injection pressure is 8 MPa, the permeability ratio initially rises and then declines, and higher injection pressures are associated with higher permeability ratios. This is because the higher injection pressures lead to the full displacement of CH_4 in the coal seam, higher desorption, and higher pore shrinkage of the coal matrix promotes the increase of coal seam permeability. CH_4 desorption decreases in the later stage of injection owing to the large amount of CO_2 absorbed in the coal seam. The swelling effect of the coal matrix is greater than the pore shrinkage and permeability decreases [43–46].

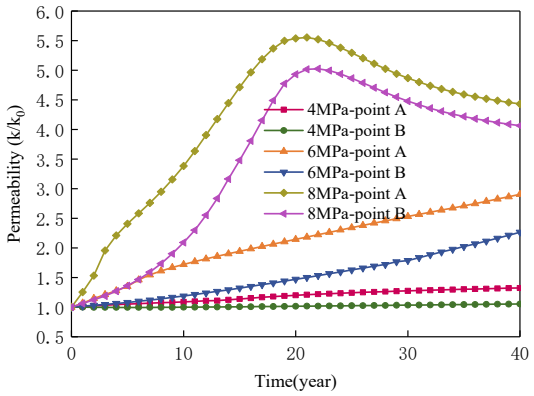

Figure 9. Permeability ratios of monitoring points at different injection pressures.

Figure 10 shows the change of permeability ratio of the monitoring points at different temperatures when the CO_2 injection pressure is 6 MPa. Permeability decreases with increasing injection temperature. This is because high temperatures increase the molecular free energy of CO_2 and CH_4, binary gas molecules become active, CO_2 is not easily adsorbed, and the expansion rate of the coal matrix decreases, leading to reduced permeability.

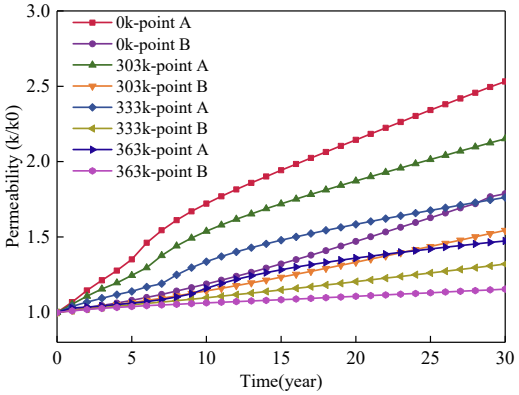

Figure 10. Permeability ratio at the monitoring points at 6 MPa and different injection temperatures.

5. Conclusions

We established a thermal–hydraulic–mechanical coupling model of binary gas seepage and diffusion and analyzed the factors influencing conventional production and CO_2-ECBM. The results are summarized as follows:

(1) Higher CO_2 injection pressure is associated with higher gas seepage velocities. CO_2 reserves and CH_4 production increase with increasing CO_2 injection pressure. When the injected CO_2 pressure is 8 MPa, the storage capacity of CO_2 is the highest, the radius of effected by CO_2 injection of 5, 10 and 30 years are 31, 44, and 58 m, respectively. After 30 years with injected CO_2 pressure of 4, 6, and 8 MPa, the productivity of CH_4 in the coal seam is 28%, 43%, and 92%, respectively. Therefore, storage of CO_2 and production of CH_4 can be significantly increased by increasing pressure.

(2) Coal seam temperature has a significant impact on CO_2-ECBM. Under the same CO_2 injection pressure, CO_2 reserves, CH_4 production, and coal seam permeability all decrease with increasing coal seam temperature. The coal seam matrix shrinks at the beginning due to the desorption of CH_4, and then it expands due to the adsorption of CO_2 and high temperature. This hinders the seepage and displacement of CO_2. Therefore, reserve of CO_2, production of CH_4, and permeability of coal seam all decrease with increasing coal seam temperature. When the injected CO_2 temperature is 363 K, the storage capacity of CO_2 is the lowest, the radius of effected by CO_2 injection of 10, 20, and 30 years are 22, 30, and 36 m, respectively. After 30 years with injected CO_2 temperature of 303, 333, and 363 K, the productivity of CH_4 in the coal seam is 25%, 22%, and 20%, respectively. The radius of effected by CO_2 injection reduces 10 m when the temperature of CO_2 injection increases from 303 to 363 K. Therefore, high temperatures are not conducive for CO_2 displacement of CH_4, and the injection temperature should be reduced.

Author Contributions: Methodology, H.L., F.C., H.J., and H.Y.; software, X.L., H.S., and H.L.; validation, F.C., H.Y., H.S., and L.X.; writing—original draft preparation, H.L. and H.Y.; writing—review and editing, H.S., H.L., H.J., H.Y., and F.C.; funding acquisition, H.L. All authors have read and agreed to the published version of the manuscript.

Funding: This research was funded by the National Science Foundation of China (51774092), the China Postdoctoral Science Foundation (2016M601399) and Guiding Projects of Daqing (ZD-2019-05).

Acknowledgments: The authors thank Tao Sun (Massachusetts Institute of Technology, USA) for his help on COMSOL application.

Conflicts of Interest: The authors declare no conflict of interest.

Abbreviations

The notations are introduced as follows:

G	The shear modulus, Pa
K	The bulk modulus of coal, Pa
E	The Young's modulus, Pa
K_S	Bulk modulus of coal skeleton
V_m	Molar constant of gas
R	Universal gas constant, J/mol·k
P_i	Gas pressure, MPa
T	Temperature of the coal, K
θ_{PY}	Stress coefficient caused by gas pressure
θ_{PX}	Stress coefficient caused by gas adsorption
θ_T	Coefficient of thermal stress
q_g	Seepage velocity(m^3/s)
J_i	Diffusion component of single phase
D_i	Diffusion coefficient of single phase, m^2/s
m_i	Gas mass of each component, kg
c_i	Molar concentration of a single component, mol/m^3
k	Permeability, m^2
Q_S	Source term, kg/(m^3·s)
M_i	Molar mass of each component, kg/mol
dQ_H	Heat source for thermal expansion
dU	The internal energy per unit volume
C_V	Specific heat at constant volume of coal seam
Q_{dis}	Differential heat source.
V_{S0}	Initial volume of coal skeleton
ΔV_S	The coal skeleton volume changes
ΔV_{SP}	Bulk expansion and deformation of coal caused by pressure
ΔV_{ST}	Bulk expansion and deformation of coal caused by temperature
k_0	The initial permeability, m^2
ν	Poisson's ratio
β	Thermal expansion coefficient, K^{-1}
δ_{ij}	Kronecker function
a_i	Langmuir volume constant, m^3/kg
b_i	Langmuir pressure constant, Pa^{-1}
ρ_c	Density of coal, kg/m^3
ε_T	Thermal expansion strain
ε_{PY}	Strain caused by gas pressure
ε_{PX}	Gas strain
ε_{ij}	Train component
u_{ij}	Displacement component
α	Biot coefficient
σ_{ij}	Stress tensor(i, j = 1, 2)
μ_i	Viscosity coefficient of single phase
ρ_i	Density of a single component, kg/m^3
φ	Porosity
ρ_a	Density of gas at standard conditions, kg/m^3
η	Thermal conductivity of coal
φ_0	Initial porosity of coal
e	Volumetric strain of coal
d_e	Effective diameter of particle

References

1. Sun, H.; Yao, J.; Gao, S.H.; Fan, D.Y.; Wang, C.C.; Sun, Z.X. Numerical study of CO_2 enhanced natural gas recovery and sequestration in shale gas reservoirs. *Int. J. Greenh. Gas Control* **2013**, *19*, 406–419. [CrossRef]
2. Xia, T.; Zhou, F.; Liu, J.; Hu, S.; Liu, Y. A fully coupled coal deformation and compositional flow model for the control of the pre-mining coal seam gas extraction. *Int. J. Rock Mech. Min. Sci.* **2014**, *72*, 138–148. [CrossRef]
3. Sobczyk, J. A comparison of the influence of adsorbed gases on gas stresses leading to coal and gas outburst. *Fuel* **2014**, *115*, 288–294. [CrossRef]
4. Zhao, Y.; Feng, Y.; Zhang, X. Selective adsorption and selective transport diffusion of CO_2–CH_4 binary mixture in coal ultramicropores. *Environ. Sci. Technol.* **2016**, *50*, 9380–9389. [CrossRef] [PubMed]
5. Orr, F.M. Onshore Geologic Storage of CO_2. *Science* **2009**, *325*, 1656–1658. [CrossRef] [PubMed]
6. Sreenivasulu, B.; Suresh, P.; Sreedhar, I.; Raghavan, K.V. Development trends in porous adsorbents for carbon capture. *Environ. Sci. Technol.* **2015**, *49*, 12641–12661. [CrossRef]
7. Shahtalebi, A.; Shukla, P.; Farmahini, A.H.; Bhatia, S.K. Barriers to diffusion of CO_2 in microporous carbon derived from silicon carbide. *Carbon* **2015**, *88*, 1–15. [CrossRef]
8. Karacan, C.; Ruiz, F.A.; Michael, C.; Phipps, S. Coal mine methane: A review of capture and utilization practices with benefits to mining safety and to greenhouse gas reduction. *Int. J. Coal Geol.* **2011**, *86*, 121–156. [CrossRef]
9. Zhou, F.; Hussain, F.; Cinar, Y. Injecting pure N_2 and CO_2 to coal for enhanced coalbed methane: Experimental observations and numerical simulation. *Int. J. Coal Geol.* **2013**, *116*, 53–62. [CrossRef]
10. Liu, J.; Xie, L.; Elsworth, D.; Gan, Q. CO_2/CH_4 Competitive Adsorption in Shale: Implications for Enhancement in Gas Production and Reduction in Carbon Emissions. *Environ. Sci. Technol.* **2019**, *53*, 9328–9336. [CrossRef]
11. Liu, X.; Wu, C.; Zhao, K. Feasibility and applicability analysis of CO_2-ECBM based on CO_2-H_2O-coal interactions. *Energy Fuels* **2017**, *31*, 9268–9274. [CrossRef]
12. Pratama, E.; Ismail, M.S.; Ridha, S. Identification of coal seams suitability for carbon dioxide sequestration with enhanced coalbed methane recovery: A case study in South Sumatera Basin, Indonesia. *Clean Technol. Environ. Policy.* **2017**, *20*, 581–587. [CrossRef]
13. Zhang, R.; Yin, X.; Winterfeld, P.H.; Wu, Y.S. A fully coupled thermal-hydrological-mechanical-chemical model for CO_2 geological sequestration. *J. Nat. Gas Sci. Eng.* **2016**, *28*, 280–304. [CrossRef]
14. Liu, J.; Xie, L.; Yao, Y.; Gan, Q.; Zhao, P.; Du, L. Preliminary study of influence factors and estimation model of the enhanced gas recovery stimulated by carbon dioxide utilization in shale. *ACS Sustain. Chem. Eng.* **2019**, *7*, 20114–20125. [CrossRef]
15. White, C.M.; Smith, D.H.; Jones, K.L.; Goodman, A.L.; Schroeder, K.T. Sequestration of carbon dioxide in coal with enhanced coalbed methane recovery a review. *Energy Fuels* **2005**, *19*, 659–724. [CrossRef]
16. Gentzis, T. Subsurface sequestration of carbon dioxide-an overview from an Alberta (Canada) perspective. *Int. J. Coal Geol.* **2000**, *43*, 287–305. [CrossRef]
17. Wu, Y.; Liu, J.; Elsworth, D.; Chen, Z.; Pan, Z. Dual poroelastic response of coal seam to CO_2 injection. *Int. J. Greenh. Gas Control* **2010**, *4*, 668–678. [CrossRef]
18. Charrière, D.; Pokryszka, Z.; Behra, P. Effect of pressure and temperature on diffusion of CO_2 and CH_4 into coal from the Lorraine basin. *Int. J. Coal Geol.* **2010**, *81*, 373–380. [CrossRef]
19. Mazumder, S.; Wolf, K.H. Differential swelling and permeability change of coal in response to CO_2 injection for ECBM. *Int. J. Coal Geol.* **2008**, *74*, 123–138. [CrossRef]
20. Wei, X.R.; Wang, G.X.; Massarotto, P.; Golding, S.D.; Rudolph, V. Numerical simulation of multicomponent gas diffusion and flow in coals for enhanced coalbed methane recovery. *Chem. Eng. Sci.* **2007**, *62*, 4193–4203. [CrossRef]
21. Fujioka, M.; Yamaguchi, S.; Nako, M. CO_2-ECBM field tests in the Ishikari Coal Basin of Japan. *Int. J. Coal Geol.* **2010**, *82*, 287–298. [CrossRef]
22. Luo, F.; Xu, R.N.; Jiang, P.X. Numerical investigation of the influence of vertical permeability heterogeneity in stratified formation and of injection/production well perforation placement on CO_2 geological storage with enhanced CH_4 recovery. *Appl. Energy* **2013**, *102*, 1314–1323. [CrossRef]

23. Vishal, V.; Singh, T.N.; Ranjith, P.G. Influence of sorption time in CO_2-ECBM process in Indian coals using coupled numerical simulation. *Fuel* **2015**, *139*, 51–58. [CrossRef]
24. Wang, G.; Ren, T.; Qi, Q.; Zhang, L.; Liu, Q. Prediction of Coalbed Methane (CBM) Production Considering Bidisperse Diffusion: Model Development, Experimental Test, and Numerical Simulation. *Energy Fuels* **2017**, *31*, 5785–5797. [CrossRef]
25. Fan, Y.; Deng, C.; Zhang, X.; Li, F.; Wang, X.; Qiao, L. Numerical study of CO_2-enhanced coalbed methane recovery. *Int. J. Greenh. Gas Control* **2018**, *76*, 12–23. [CrossRef]
26. Fang, H.H.; Sang, S.X.; Liu, S.Q. Numerical simulation of enhancing coalbed methane recovery by injecting CO_2 with heat injection. *Pet. Sci.* **2019**, *16*, 32–43. [CrossRef]
27. Fan, C.; Elsworth, D.; Li, S.; Zhou, L.; Yang, Z.; Song, Y. Thermo-hydro-mechanical-chemical couplings controlling CH_4 production and CO_2 sequestration in enhanced coalbed methane recovery. *Energy* **2019**, *173*, 1054–1077. [CrossRef]
28. Li, H.; Lin, B.; Yang, W.; Hong, Y.; Wang, Z. A fully coupled electromagnetic-thermal-mechanical model for coalbed methane extraction with microwave heating. *J. Nat. Gas Sci. Eng.* **2017**, *46*, 830–844. [CrossRef]
29. Fan, C.; Elsworth, D.; Li, S.; Chen, Z.; Luo, M.; Song, Y.; Zhang, H. Modelling and optimization of enhanced coalbed methane recovery using CO_2/N_2 mixtures. *Fuel* **2019**, *253*, 1114–1129. [CrossRef]
30. Li, S.; Fan, C.; Han, J.; Luo, M.; Yang, Z.; Bi, H. A fully coupled thermal-hydraulic-mechanical model with two-phase flow for coalbed methane extraction. *J. Nat. Gas Sci. Eng.* **2016**, *33*, 324–336. [CrossRef]
31. Teng, T.; Zhao, Y.; Gao, F.; Wang, J.G.; Wang, W. A fully coupled thermo-hydro-mechanical model for heat and gas transfer in thermal stimulation enhanced coal seam gas recovery. *Int. J. Heat Mass Transf.* **2018**, *125*, 866–875. [CrossRef]
32. Xia, T.; Zhou, F.; Gao, F.; Kang, J.; Liu, J.; Wang, J. Simulation of coal self-heating processes in underground methane-rich coal seams. *Int. J. Coal Geol.* **2015**, *141*, 1–12. [CrossRef]
33. Liu, J.; Chen, Z.; Elsworth, D.; Qu, H.; Chen, D. Interactions of multiple processes during CBM extraction: A critical review. *Int. J. Coal Geol.* **2011**, *87*, 175–189. [CrossRef]
34. Qu, H.; Liu, J.; Chen, Z.; Wang, J.; Pan, Z.; Connell, L. Complex evolution of coal permeability during CO_2 injection under variable temperatures. *Int. J. Greenh. Gas Control* **2012**, *9*, 281–293. [CrossRef]
35. Huang, S.P. In situ stress distribution and its impact on CBM reservoir properties in the Zhengzhuang area, southern Qinshui Basin, North China. *J. Nat. Gas Sci. Eng.* **2019**, *61*, 83–96. [CrossRef]
36. Zhang, H.; Liu, J.; Elsworth, D. How sorption-induced matrix deformation affects gas flow in coal seams: A new FE model. *Int. J. Rock Mech. Min. Sci.* **2008**, *45*, 1226–1236. [CrossRef]
37. Liu, T.; Lin, B.; Yang, W.; Liu, T.; Kong, J.; Huang, Z. Dynamic diffusion-based multifield coupling model for gas drainage. *J. Nat. Gas Sci. Eng.* **2017**, *44*, 233–249. [CrossRef]
38. Zhu, W.C.; Wei, C.H.; Liu, J.; Qu, H.Y.; Elsworth, D. A model of coal–gas interaction under variable temperatures. *Int. J. Coal Geol.* **2011**, *86*, 213–221. [CrossRef]
39. Liu, Z.; Cheng, Y.; Liu, Q.; Jiang, J.; Li, W.; Zhang, K. Numerical assessment of CMM drainage in the remote unloaded coal body: Insights of geostress-relief gas migration and coal permeability. *J. Nat. Gas Sci. Eng.* **2017**, *45*, 487–501. [CrossRef]
40. Kong, X.; Wang, E.; Liu, Q.; Li, Z.; Li, D.; Cao, Z. Dynamic permeability and porosity evolution of coal seam rich in CBM based on the flow-solid coupling theory. *J. Nat. Gas Sci. Eng.* **2017**, *40*, 61–71. [CrossRef]
41. Li, X.C.; Guo, Y.Y.; Wu, S.Y.; Nie, B.S. Mathematical model and numerical simulation of fluid-solid coupled flow of coal-bed gas considering swelling stress of adsorption. *Chin. J. Rock Mech. Eng.* **2007**, *26*, 2743–2748.
42. Zheng, C.; Chen, Z.; Kizil, M.; Aminossadati, S.; Zou, Q.; Gao, P. Characterisation of mechanics and flow fields around in-seam methane gas drainage borehole for preventing ventilation air leakage: A case study. *Int. J. Coal Geol.* **2016**, *162*, 123–138. [CrossRef]
43. Pan, Z.; Connell, L.D. Comparison of adsorption models in reservoir simulation of enhanced coalbed methane recovery and CO_2 sequestration in coal. *Int. J. Greenh. Gas Control* **2009**, *3*, 77–89. [CrossRef]
44. Balan, H.O.; Gumrah, F. Assessment of shrinkage–swelling influences in coal seams using rank-dependent physical coal properties. *Int. J. Coal Geol.* **2009**, *77*, 203–213. [CrossRef]

45. Durucan, S.; Shi, J.Q. Improving the CO_2 well injectivity and enhanced coalbed methane production performance in coal seams. *Int. J. Coal Geol.* **2009**, *77*, 214–221. [CrossRef]
46. Han, L.F.; Hou, Y.D.; Wang, Y.J.; Liu, X.B.; Han, J.; Xie, R.H.; Mu, H.W.; Fu, C.F. Measurement of Velocity of Sand -Containing Oil–Water Two-Phase Flow with Super High Water Holdup in Horizontal Small Pipe Based on Thermal Tracers. *Flow Meas Instrum.* **2019**, *69*, 101622–101631. [CrossRef]